Direction-dependent tunneling through nanostructured magnetic barriers in graphene

M. Ramezani Masir,[1] P. Vasilopoulos,[2,*] A. Matulis,[3,†] and F. M. Peeters[1,‡]
[1]*Department of Physics, University of Antwerp, Groenenborgerlaan 171, B-2020 Antwerpen*
[2]*Department of Physics, Concordia University, Montreal, Quebec, Canada H3G 1M8*
[3]*Semiconductor Physics Institute, Gostauto 11, 2600 Vilnius, Lithuania*
(Received 25 March 2008; revised manuscript received 23 May 2008; published 27 June 2008)

We evaluate the transmission through magnetic barriers in graphene-based nanostructures. Several particular cases are considered: a magnetic step, single and double barriers, and δ-function barriers. A separate class of magnetic-barrier structures are those with inhomogeneous magnetic-field profiles, such that the average magnetic field vanishes, which can be realized by nanostructured ferromagnetic stripes placed on top of the graphene layer. Quantum bound states that are localized near or in the barrier are predicted for a magnetic step and some structures with finite-width barriers but none for δ-function barriers. When a bound state is localized close to the barrier edge, it has a nonzero velocity parallel to this edge. The transmission depends strongly on the direction of the incident electron or hole wave vector and gives the possibility to construct a direction-dependent wave vector filter. In general, the resonant structure of the transmission is significantly more pronounced for (Dirac) electrons with *linear* spectrum than for the usual electrons with a *parabolic* spectrum.

DOI: 10.1103/PhysRevB.77.235443 PACS number(s): 71.10.Pm, 73.21.−b, 81.05.Uw

I. INTRODUCTION

The recent realization of stable single-layer carbon crystals, called graphene, as well as that of multilayer graphene has led to an intensive investigation of graphene's electronic properties.[1,2] Charge carriers in a wide single-layer graphene behave like "relativistic" chiral massless particles with a "light speed" equal to the Fermi velocity and possess a gapless linear spectrum close to the K and K' points.[1,3] One major consequence is that single-layer graphene displays an unconventional quantum Hall effect (QHE), in which the plateaus occur[4] at half-integer multiples of $4e^2/h$. An equally unconventional QHE occurs in bilayer graphene.[5] Another one is the perfect transmission through arbitrarily high and wide barriers, referred to as Klein tunneling.[6–9] These properties and the submicron long mean-free paths[1] may have important consequences for the design of graphene-based devices (see Ref. 10 for recent reviews).

To circumvent the Klein tunneling and produce confined graphene-based structures, pertinent, e.g., to quantum computing and the design of devices in general, various schemes have been proposed: single-layer graphene strips,[11] gated nanoribbons,[12] gated and/or doped bilayers,[9,13] etc. Another approach exploits the inherently two-dimensional (2D) motion through magnetic barriers initiated in Ref. 14 and recently applied to graphene, with a single magnetic barrier, in Ref. 15 and double barrier in Ref. 16. Here, using a considerable experience we acquired on motion through inhomogeneous magnetic fields[17] B, we build on and significantly extend the latter approach by considering double and multiple magnetic barriers, δ-function barriers, and barriers with a magnetic-field profile in which B is reversed once or a few times within the same structure. The latter magnetic profile can be realized by ferromagnetic stripes[14] put on top of the graphene layer. Recently,[18] edge states were studied in graphene in a nonuniform magnetic field.

The paper is organized as follows. In Sec. II we evaluate the energy spectrum of a 2D graphene layer in a homogeneous magnetic field and give the formula for the ballistic conductance. In Sec. III we evaluate the spectrum pertinent to a magnetic step and the electron velocity parallel to it. In Sec. IV we evaluate the transmission through single and double magnetic barriers, and in Sec. V that through complex structures with vanishing average magnetic field as well as various δ-function barriers. We make concluding remarks in Sec. VI.

II. BASIC FORMALISM

A. Homogenous magnetic field

An electron in a single graphene layer, in the presence of perpendicular magnetic field $B(x)$, which may vary along the x direction, is described by the Hamiltonian

$$H_0 = v_F \boldsymbol{\sigma} \cdot (\mathbf{p} + e\mathbf{A}(x)), \tag{1}$$

where $\mathbf{p}$ is the momentum operator, v_F is the Fermi velocity, and $\mathbf{A}(x)$ is the vector potential. Here we first present results for a homogeneous magnetic field B_0, with $\mathbf{A}(x) = (0, B_0 x, 0)$, and will contrast them later with those for inhomogeneous magnetic fields. To simplify the notation we introduce the dimensionless units: $\ell_B = [\hbar/eB_0]^{1/2}$, $B(x) \to B_0 B(x)$, $A(x) \to B_0 \ell_B A(x)$, $t \to t\ell_B/v_F$, $\vec{r} \to \ell_B \vec{r}$, $\vec{v} \to v_F \vec{v}$, $E \to E_0 E$, $E_0 = \hbar v_F/\ell_B$. In these units Eq. (1) is written explicitly as

$$H = -\mathrm{i}\begin{pmatrix} 0 & \partial_x - \mathrm{i}\partial_y + x \\ \partial_x + \mathrm{i}\partial_y - x & 0 \end{pmatrix}. \tag{2}$$

Then the equation $H\Psi(x,y) = E\Psi(x,y)$ admits solutions

$$\Psi(x,y) = \begin{pmatrix} \psi_I(x,y) \\ \psi_{II}(x,y) \end{pmatrix}, \tag{3}$$

with $\psi_I(x,y)$ and $\psi_{II}(x,y)$ obeying the coupled equations,

$$i[\partial/\partial x - \mathrm{i}\,\partial/\partial y + x]\psi_{II} + E\psi_I = 0, \tag{4a}$$

$$i[\partial/\partial x + \mathrm{i}\,\partial/\partial y - x]\psi_I + E\psi_{II} = 0. \tag{4b}$$

Due to the translational invariance along the y direction, we assume solutions of the form $\Psi(x,y) = \exp(ik_y y)[a(x), \ b(x)]^T$, T denoting the transpose of the row vector. Then Eqs. (4a) and (4b) take the form

$$-i[d/dx + (k_y + x)]b = Ea, \tag{5a}$$

$$-i[d/dx - (k_y + x)]a = Eb. \tag{5b}$$

Operating on Eqs. (5a) and (5b) with $-i[d/dx-(k_y+x)]$ gives

$$[d^2/dx^2 - (k_y + x)^2 \mp 1 + E^2]c_\mp = 0, \tag{6}$$

where $c_- = a$ and $c_+ = b$. The solution of Eq. (6) are the well-known Hermite polynomials $H(x)$. For $c_- = a$ the wave function is $a(x) = \exp(-z^2/4)H_{E^2/2-1}(x+k_y)$ and the energy spectrum is

$$E_n = \pm\sqrt{2(n+1)}. \tag{7}$$

Repeating this procedure for $c_+ = b$ gives $b(x) = \exp(-z^2/4)H_{E^2/2}(x+k_y)$ with spectrum

$$E_n = \pm\sqrt{2n}. \tag{8}$$

Notice the difference of these spectra from the one for the usual electrons $E_n = \hbar\omega_c(n+1/2)$. The solution of Eq. (6) can also be written as a linear combination of the Weber functions $D_p(z)$ and $D_{p-1}(z)$ with $z = \sqrt{2}(x+k_y)$; as such it is more suitable for the case of inhomogeneous magnetic fields and will be used in Secs. III and IV.

B. Conductance

We will also calculate the conductance G for various magnetic-barrier structures by introducing it as the electron flow averaged over half the Fermi surface,[14]

$$G = G_0 \int_{-\pi/2}^{\pi/2} T(E_F, E_F \sin\phi)\cos\phi \ d\phi. \tag{9}$$

Here ϕ is the angle of incidence relative to the x direction, and $G_0 = 2e^2 E_F \ell/(\pi h)$. For electrons with parabolic spectrum $E_F \sin\phi$ should be replaced by $\sqrt{E_F}\sin\phi$ and $G_0 = e^2 m v_F \ell/\hbar^2$, where ℓ is the length of the structure along the y direction and v_F the Fermi velocity. $T(x,y)$ is the transmission through the studied structure.

III. MAGNETIC FIELD STEP

A. General case

We consider a region $x<0$, in which there is no magnetic field followed by one $x>0$ in which there is a constant magnetic field B. This is formally described by

$$B(x) = B\Theta(x) \tag{10}$$

and was previously studied in Ref. 15. For completeness we repeat the essential steps to find bound states close to the magnetic-field step. In Sec. II we obtained the electron wave function in a constant magnetic field for $x>0$. We have to match this wave function with that of a free electron for $x<0$.

For a free electron the term $+x$ in Eqs. (5a) and (5b) is absent and the wave-function components a and b obey

$$Ea + i(d/dx + k_y)b = 0, \tag{11a}$$

$$i(d/dx - k_y)a + Eb = 0. \tag{11b}$$

Assuming exponential solutions $a, \ b \propto e^{ik_x x}$ Eqs. (11a) and (11b) become two linear algebraic equations. Equating to zero the determinant of their coefficients gives

$$E^2 = k_x^2 + k_y^2, \tag{12}$$

with $k_x \pm ik_y = (k_x^2+k_y^2)^{1/2}\exp(\pm i\varphi) = E\exp(\pm i\varphi)$. For $E^2 - k_y^2 > 0$ the general solution is

$$a(x) = fe^{ik_x x} + ge^{-ik_x x}, \tag{13a}$$

$$b(x) = fe^{ik_x x + i\varphi} - ge^{-ik_x x - i\varphi}, \tag{13b}$$

while for $E^2 - k_y^2 < 0$, the solution is

$$a(x) = S_+ fe^{k_x x} + S_- ge^{-k_x x}, \tag{14a}$$

$$b(x) = fe^{k_x x} + ge^{-k_x x}, \tag{14b}$$

with $S_\pm = -i(\pm k_x + k_y)/E$.

To properly match the solution for $x<0$ to that for $x>0$ at the step, we write the solutions for $x>0$ as a linear combination of Weber functions $D_p(x)$ and $D_{p-1}(x)$. With $p = E^2/2$ and $z = \sqrt{2}(x+k_y)$, this gives

$$b = CD_p(z), \tag{15a}$$

$$a = -iC(E/\sqrt{2})D_{p-1}(z). \tag{15b}$$

Here C is a constant. Then matching the wave functions at $x=0$ gives

$$f - CD_{p-1}(\sqrt{2}k_y) = 0, \tag{16}$$

$$S_+ f + iC(E/\sqrt{2})D_p(\sqrt{2}k_y) = 0. \tag{17}$$

Setting to zero the determinant of the coefficients gives the spectrum E as a function of k_y by solving

$$(\sqrt{2}(k_x + k_y)/E)D_p(\sqrt{2}k_y) = ED_{p-1}(\sqrt{2}k_y). \tag{18}$$

Numerical results are shown in Fig. 1(a) and are identical to those of Ref. 15, except for the $n=0$ level ($E=0$), which was absent in Ref. 15. Note that we have an infinite number of bound states labeled by the Landau-level index n in the $B>0$ region. For $k_y \ll -1/\ell_B$ the center of the electron orbit $\langle x\rangle = -k_y$ is located deep in the magnetic region ($B>0$) and the electron feels a homogeneous magnetic field. Then the bound state corresponds to the Landau level with energy $E = \pm\sqrt{2n}$. On the other hand, for $k_y\ell_B \to 0$ the spectrum approaches the free-electron spectrum in graphene, shown by the dashed orange line, since the center of the orbit comes closer and closer to the $B=0$ region. This corresponds to the standard electron case discussed in Ref. 14 with the line $E = \pm\hbar v_F k_y$ replaced by the free-electron parabola.

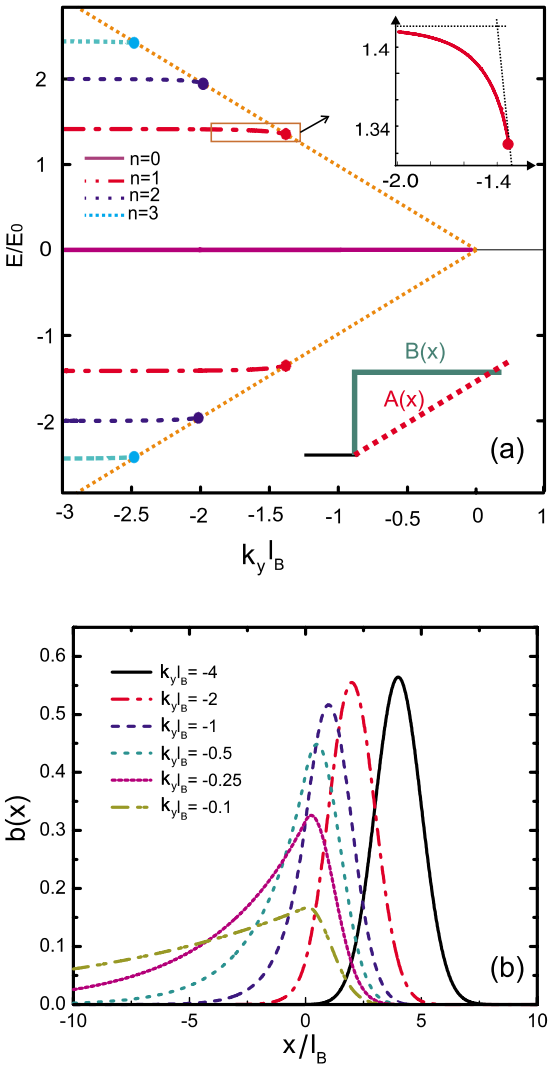

FIG. 1. (Color online) (a) Bound states energy spectrum vs the wave-vector component (k_y) parallel to the magnetic step. The orange dashed line is the free-electron spectrum $E=\pm\hbar v_F k_y$. The upper inset shows a zoom of the $n=1$ state near $E=k_y\hbar v_F$. The lower inset shows the magnetic-field and vector potential profiles. (b) Wave function $b(x)$ for the $E=0$ level for different values of the momentum k_y.

B. Zero energy problem

The case $E=0$ cannot be treated as outlined above and therefore was missed in Ref. 14. We assume $E=0$ in Eqs. (5a) and (5b) and check if a bound state exists. Integrating these first-order differential equations gives

$$a = C_1 e^{(x+k_y)^2/2}, \quad b = C_2 e^{-(x+k_y)^2/2}. \tag{19}$$

The solution for b is acceptable: it vanishes for $x\to+\infty$, and consequently, it is the wave function of a bound state. The solution for a is not acceptable as it is not confined and therefore $C_1=0$. For $x>0$ the resulting eigenfunction corresponding to the zero Landau level reads

$$\Psi = e^{ik_y y} e^{-(x+k_y)^2/2} \begin{pmatrix} 0 \\ 1 \end{pmatrix}, \tag{20}$$

and the corresponding eigenvalue is $E=0$.

Let us consider the $x<0$ region where $B=0$. The spectrum of a free electron is continuous with a peculiar point $E=0$ also called the Dirac point. This becomes important when we construct bound-state eigenfunctions in magnetic-barrier structures. That is why we consider this eigenfunction in more detail below. Inserting $E=0$ and a and $b\propto e^{ik_x x}$ in Eqs. (11a) and (11b) we obtain

$$(k_x - ik_y)b = 0, \tag{21a}$$

$$(k_x + ik_y)a = 0. \tag{21b}$$

A homogeneous wave function is obtained only if the momentum is zero, that is, only for $k_x=k_y=0$. Then the wave-function components can have any value. However, if we are looking for a wave function only in some part of the xy plane, say, in the region $x<0$, one more solution is possible, namely, one for $a=0$ and $b\neq 0$. Then Eq. (21a) gives $k_x=ik_y$. Thus, for $k_y<0$ we have

$$\Psi = e^{ik_y y} e^{|k_y|x} \begin{pmatrix} 0 \\ 1 \end{pmatrix}. \tag{22}$$

This is exactly what we need for matching it with the function (20) in the magnetic-field region ($x>0$). As Eqs. (20) and (22) have only a single b component, the boundary condition can be satisfied by just choosing a proper coefficient. Thus, we have a bound state with zero energy as long as the momentum k_y is negative. When k_y vanishes, k_x is not positive any more: this means that an electron can escape to $-\infty$ and the bound state disappears. Numerical results for the wave function are given in Fig. 1(b) and show clearly the increased leakage of the electron wave function into the magnetic-barrier region for $-k_y\to 0$.

C. Electron velocity

The bound states discussed above are bound only in the direction perpendicular to the magnetic step, i.e., they are localized close to the step but the electron (or hole) may propagate along the magnetic step, i.e., along the y direction. Below we evaluate the average velocity along the magnetic step $v_n(k_y)$. We operate on Eqs. (5a) and (5b) for $x>0$ and on Eqs. (11a) and (11b) for $x<0$, with $\partial/\partial k_y$ and integrate over x. The result is

$$-ia^* b = a^* a(\partial E/\partial k_y), \tag{23a}$$

$$ib^* a = b^* b(\partial E/\partial k_y) \tag{23b}$$

and gives

$$v_n(k_y) = \partial E/\partial k_y = \int_{-\infty}^{+\infty} dx j_y(x), \tag{24}$$

where $j_y=-i(a^*b-b^*a)$. Numerical results for $v_n(k_y)$ are shown in Fig. 2 for various bound states. Notice that the

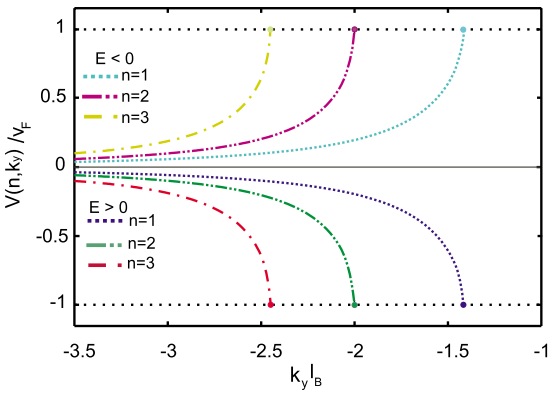

FIG. 2. (Color online) Average electron ($E>0$) and hole ($E<0$) velocities along the magnetic step. The different bound states are labeled by the Landau-level index n.

electron and hole bound states have opposite velocities and consequently the direction of their current flow is the same. At the k_y value for which the bound state disappears the carrier attains the Fermi velocity, i.e., the velocity of an unbound particle in graphene.

IV. SIMPLE BARRIER STRUCTURES

A. Single barrier

We consider a magnetic barrier in the region $-d/2<x<d/2$, as shown in the inset of Fig. 4. For $x<d/2$, $-d/2<x<d/2$, and $x>d/2$, the Hamiltonian is given by Eq. (2) with the upper (lower) off-diagonal elements shifted, respectively, by $-d/2$ $(d/2)$, x $(-x)$, and $d/2$ $(-d/2)$. Proceeding as in Sec. II we obtain for $x<d/2$

$$(d^2/dx^2 - q_-^2 + E^2)c = 0, \tag{25}$$

where $q_-=k_y-d/2$ and $c=a$ and b. By setting $k_x^2=E^2-q_-^2$ and $\tan\phi_1=q_-/k_x$, the solution for Ψ is

$$\Psi_1 = \begin{pmatrix} e^{ik_x x} + re^{-ik_x x} \\ e^{ik_x x+i\phi_1} - re^{-ik_x x-i\phi_1} \end{pmatrix}. \tag{26}$$

For $-d/2<x<d/2$ we have again Eq. (6). The corresponding solution is a linear combination of Weber functions,

$$\Psi_2 = \begin{pmatrix} C_1 D_{p-1}(z) + C_2 D_{p-1}(-z) \\ (i\sqrt{2}/E)[C_1 D_p(z) - C_2 D_p(-z)] \end{pmatrix}, \tag{27}$$

where $z=\sqrt{2}(x+k_y)$ and $p=E^2/2$. Finally, for $x>d/2$ we define $\tan\phi_2=q_+/k_2$, $q_+=k_y+d/2$, and $k_x'^2=E^2-q_+^2$. Then the wave function takes the form

$$\Psi_3 = . \begin{pmatrix} te^{ik_x' x} \\ te^{ik_x' x+i\phi_2} \end{pmatrix}. \tag{28}$$

Matching the solutions and the flux at $x=-d/2$ and $x=d/2$ gives the transmission probability T. Setting $\alpha_1=e^{-ik_x d/2}$, $\alpha_2=e^{ik_x d/2}$, $\alpha_3=D(p-1,\sqrt{2}q_-)$, $\alpha_4=D(p-1,-\sqrt{2}q_-)$, $\gamma_1=(i\sqrt{2}/E)D(p,\sqrt{2}q_-)$, $\gamma_2=(i\sqrt{2}/E)D(p,-\sqrt{2}q_-)$, $\omega_1=D(p-1,\sqrt{2}q_+)$, $\omega_2=D(p-1,-\sqrt{2}q_+)$, $\eta_1=(i\sqrt{2}/E)D(p,\sqrt{2}q_+)$, $\eta_2=(i\sqrt{2}/E)D(p,-\sqrt{2}q_+)$, and $\gamma_3=e^{ik_x' d/2}$, the result for t is

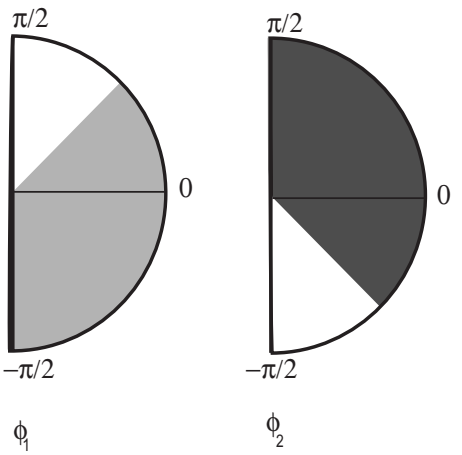

FIG. 3. Schematics for the ranges of the possible angles of incidence ϕ_1 and angles of exit ϕ_2 for which electrons are able to propagate through the magnetic barrier.

$$t = \frac{2(\eta_2\omega_1 + \eta_1\omega_2)\alpha_1 \cos\phi_1}{\gamma_3[f^+g^+ - f^-g^-]}, \tag{29}$$

where $f^+=\eta_2+\omega_2 \exp i\phi_2$, $f^-=\eta_1-\omega_1 \exp i\phi_2 g^+=\gamma_1+\alpha_3 \exp -i\phi_1$, and $g^-=\gamma_2-\alpha_4 e \exp -i\phi_1$. Then

$$T = (k_x'/k_x)|t|^2, \tag{30}$$

where the factor k_x'/k_x is due to current conservation. From $k_x=[E^2-(k_y-d/2)^2]^{1/2}$ we have the range of k_y values $-E+d/2\le k_y\le E+d/2$, and from $k_x'=[E^2-(k_y+d/2)^2]^{1/2}$, the range $-E-d/2\le k_y\le E-d/2$. This means that the acceptable range of k_y values, for which the transmission result (30) holds, is

$$-E+d/2 \le k_y \le E-d/2. \tag{31}$$

Since $k_y=E\sin\phi_1+d/2=E\sin\phi_2-d/2$, Eq. (31) gives the ranges for the angles ϕ_1 and ϕ_2, shown in Fig. 3,

$$-1 \le \sin\phi_1 \le 1-d/E, \tag{32a}$$

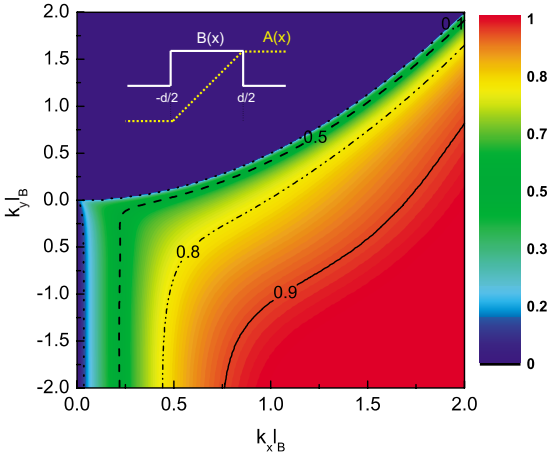

FIG. 4. (Color online) Contour plot of the transmission T through a magnetic barrier of width $d=l_B$. The inset shows the corresponding magnetic-field and vector potential profiles.

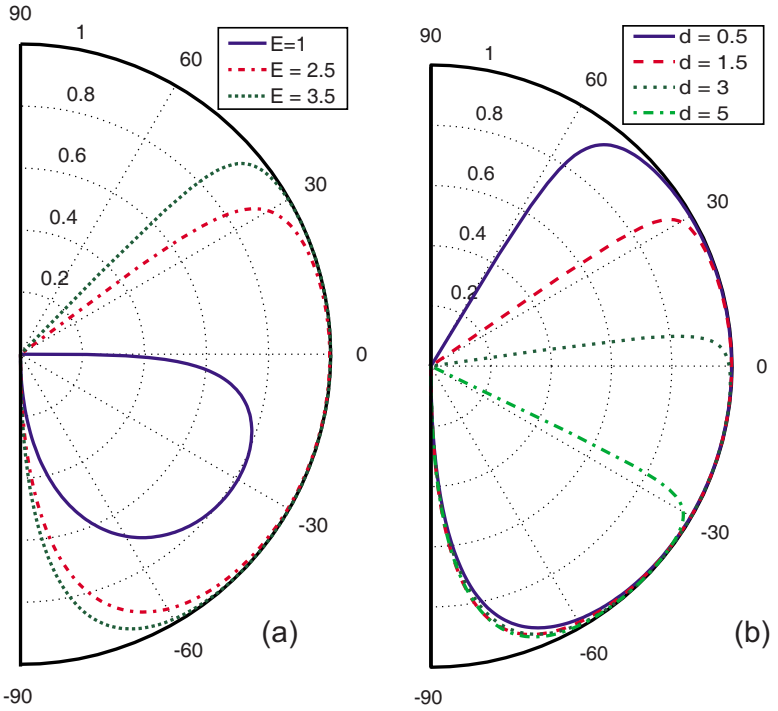

FIG. 5. (Color online) (a) Angular dependence of the transmission through a barrier of width $d=l_B$ for different values of the electron energy. (b) As in (a) for an electron with energy $E=3.5E_0$ and different barrier widths.

$$-1+d/E \leq \sin\phi_2 \leq 1. \tag{32b}$$

These ranges depend on d/E. The transmission is nonzero only for ϕ_1 and ϕ_2 in these ranges and vanishes for $d \geq 2E$. For standard electrons Eq. (32a) and (32b) holds but with d/E replaced by $d/(2E)^{1/2}$.

A contour plot of the transmission coefficient is shown in Fig. 4 for a magnetic barrier with width $d=l_B$. Note that the transmission coefficient depends not only on the value of the momentum perpendicular to the magnetic barrier but also on the carrier momentum parallel to it. The boundary of the $T=0$ region is well approximated by the classical result: $k_y=k_x^2/2d$. The angular dependence of T is made more clear in Fig. 5 where it is shown for different angles of incidence.

The spectrum of bound states is determined by

$$F^-(q_-)G^+(-q_+)-F^+(q_+)G^-(-q_-)=0, \tag{33}$$

with $F^{\pm}(z)=D_{p-1}(z)-(i\sqrt{2}/ES_{\pm})D_p(z)$, $G^{\pm}(z)=D_{p-1}(z)+(i\sqrt{2}/ES_{\pm})D_p(z)$, and $S_{\pm}=(i/E)[q_- \mp (q_-^2-E^2)^{1/2}]$. The dispersion relation (33) for $d=5\ell_B$ is shown in Fig. 6 as a function of k_y. For $k_y>0$ the bound states are localized near the $x\approx -d/2$ edge while for $k_y<0$ they are localized near the $x\approx d/2$ edge. There are seven bound states in Fig. 6 delimited by the free-electron spectrum $E=\pm\hbar v_F k_y$ (blue dashed lines). Notice that those for $n\neq 0$ have a nonzero velocity for energies different from the Landau levels $E=\pm\sqrt{2nE_0}$. The number of bound states n decreases with the width of the

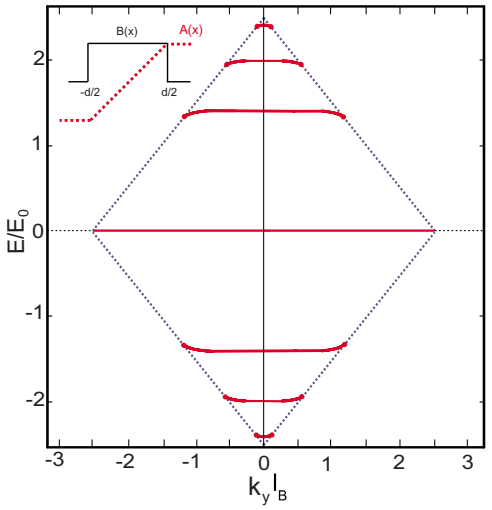

FIG. 6. (Color online) Energy spectrum E of the bound states as a function of k_y for a magnetic barrier of width $d=5l_B$. Inset: magnetic-field and vector potential profiles.

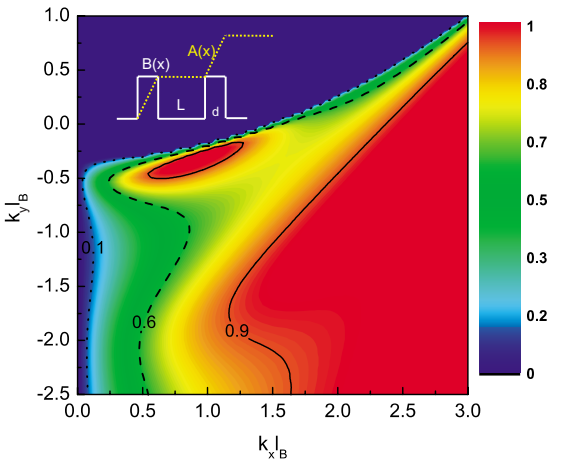

FIG. 7. (Color online) Contour plot of the transmission T through a double magnetic barrier with $d=l_B$ and $L=3l_B$. The inset shows the magnetic-field and vector potential profiles.

barrier but it is independent of its height. For $d<1.3\ \ell_B$ only the $E=0$ level is left as bound state.

B. Double barrier

We consider now a resonant tunneling structure, i.e., a double magnetic barrier shown in the inset of Fig. 7. The vector potential is given by

$$A=\begin{cases}0, & x<-L/2-d\\ 1/d[x+(L/2+d)], & -L/2-d\le x\le -L/2\\ 1, & -L/2<x<L/2\\ 1/d[x-(L/2-d)], & L/2\le x\le L/2+d\\ 2, & x>L/2+d\end{cases}. \tag{34}$$

Using Eq. (1) the procedure of Sec. IV A is repeated in a straightforward manner and the transfer-matrix technique gives the transmission probability. The resulting expressions are very lengthy; here we will give only the numerical results. In Fig. 7 we show a contour plot of the transmission probability as a function of k_x and k_y. As compared to a single barrier (see Fig. 4), the transmission exhibits a more pronounced structure. This is made clear in Fig. 8 upon comparing the inset with the main figure. The double barrier exhibits clear resonances that are absent in the single barrier. Notice that for electrons with a parabolic spectrum the resonances occur at different values of k_x and are much weaker. The transmission depends strongly on the angle of incidence as made explicit in Fig. 9. In Fig. 9(a) we considered $d=l_B$ and $L=2l_B$ and changed the energy while in Fig. 9(b) we fixed the energy $E=3E_0$ and the distance between two barriers $L=2l_B$ and changed the length of the barrier.

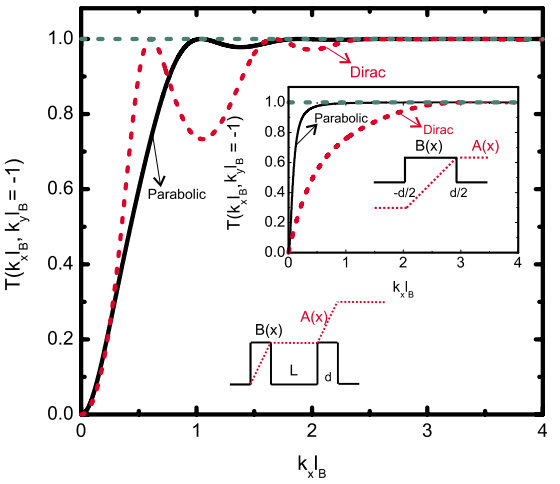

FIG. 8. (Color online) Transmission T through a double magnetic barrier for Dirac electrons (dashed red curve) and standard electrons (solid black curve) with $d=l_B$ and $L=3l_B$. The upper inset shows the corresponding results for a single magnetic barrier.

C. Structures with $\langle B\rangle=0$

In line with previous studies for standard electrons[17] and in search for more pronounced resonances, below we consider complex graphene structures with $\langle B\rangle=0$ and compare their transmission probability and conductance with those for standard electrons with a parabolic energy spectrum. In Fig. 10 we show a contour plot of the transmission probability for the complex structure shown in its inset. Such a magnetic-field profile is a simple model for a strip magnetized perpendicular to the graphene[14] layer. Compared to the single-barrier structure of Fig. 4, the transmission is now symmetric with respect to $k_y\to -k_y$ and exhibits a resonance behavior. When the strip is magnetized parallel to the layer but perpen-

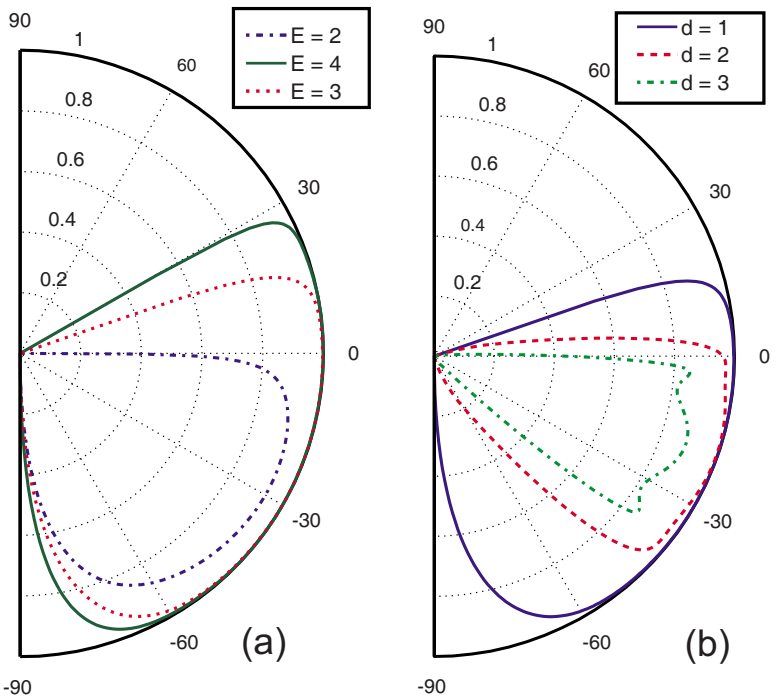

FIG. 9. (Color online) (a) Angular dependence of the transmission through a double magnetic barrier for $d=l_B$, $L=2l_B$, and different electron energies. (b) As in (a) for $E=3E_0$, $L=2l_B$, and different values of d.

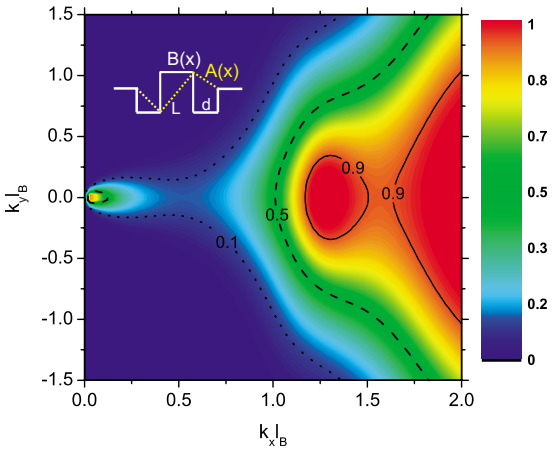

FIG. 10. (Color online) Contour plot of the transmission T through a complex magnetic-barrier structure, shown in the inset, with $\langle B\rangle=0$, well width $d=l_B$, and barrier width $L=2l_B$.

dicular to the magnetic strip, the magnetic-field profile can be modeled by that given in the inset of Fig. 11. The corresponding contour plot of the transmission probability is shown in Fig. 11 for $d=l_B$.

Next we will use the above units to construct new resonant tunneling structures. In Fig. 12 we use the complex unit of Fig. 10 to build the structure with the field and corresponding vector potential profiles shown in its inset. The transmission exhibits strong resonances that are shown more clearly in Fig. 13. The resonances are more pronounced for Dirac electrons than for the usual electrons. Another resonant structure we can build with the unit of Fig. 11 is shown in the inset of Fig. 14. The corresponding contour plot of the transmission is shown in Fig. 14; it exhibits strong resonances along k_x and to a lesser extent along k_y. A comparison with standard electrons is made in Fig. 15. Notice the much more pronounced resonances for massless Dirac electrons in Figs. 13 and 15 despite the similarity of Figs. 12 and 14 to Fig. 5 of Ref. 14. In fact, the perfect transmission regions in Figs. 12 and 14 are much narrower than those in Fig. 5 of Ref. 14.

We have also calculated the conductance G for these two structures, using Eq. (9), and compared it with that for standard electrons. In Figs. 16(a) and 16(b) we plot G as a function of the energy. The conductance is a quantity easier to measure than the momentum-dependent transmission coefficient. The resonances in G, similar to those in the transmission, are more pronounced for Dirac electrons than for the usual electrons.

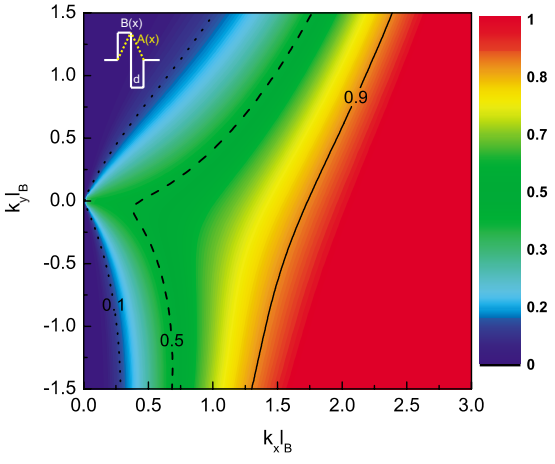

FIG. 11. (Color online) Contour plot of the transmission T through a complex magnetic-barrier structure (see inset) with $\langle B\rangle=0$ and barrier and/or well width $d=l_B$.

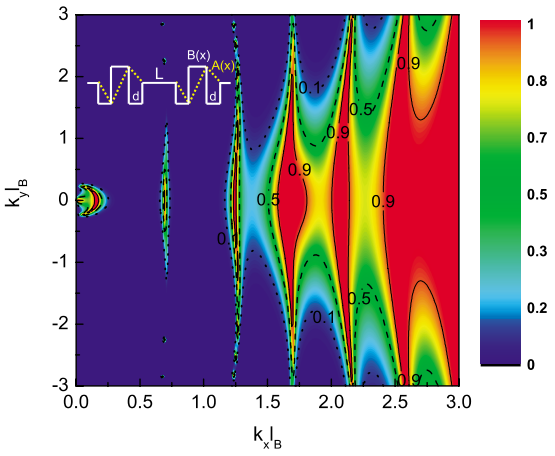

FIG. 12. (Color online) Contour plot of the transmission T through the complex structure shown the inset with $\langle B\rangle=0$, barrier width $d=l_B$, and well width $L=3l_B$.

D. Delta-function magnetic barriers

Analytical results for the transmission coefficient can be obtained if we consider δ-function barriers.[19] Below we give the main results for single and double barriers. For a *single* magnetic δ-function barrier, we have $B(x)=B_0 l_B \delta(x)$; the corresponding vector potential is $A(x)=B_0 l_B[\theta(x)-\theta(-x)]/2$, where $\theta(x)$ is the step function. For the chosen gauge k_y is a constant of motion and the wave function has the form $\Psi(x,y)=e^{ik_y y}\psi(x)$.

In the dimensionless units of Sec. II the solution of the Schrödinger equation for a standard electron is

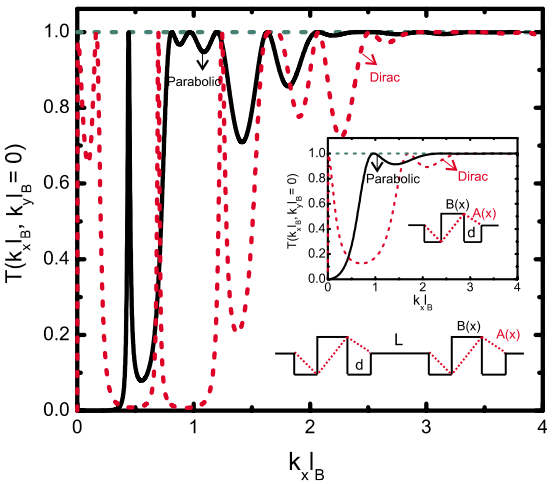

FIG. 13. (Color online) Transmission probability for a Dirac electron and a standard electron. The two-unit structure shown in the lower inset has $d=l_B$ and $L=3l_B$. The upper inset shows the corresponding result through a single unit.

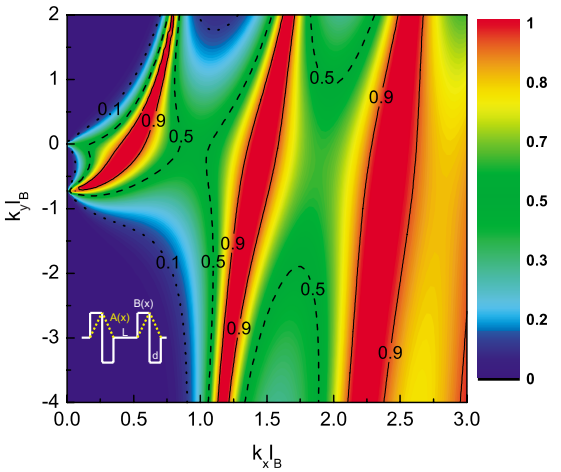

FIG. 14. (Color online) Contour plot of the transmission through a two-unit resonant structure with $\langle B\rangle=0$, $d=0.5l_B$, and $L=3l_B$. The single unit is shown in Fig. 11.

$$\psi(x)=\begin{cases} e^{ik_x x}+re^{-ik_x x} & x<0 \\ te^{ik_x' x} & x>0. \end{cases} \tag{35}$$

This results in the transmission probability

$$T=|t|^2(k_x'/k_x), \tag{36}$$

where $t=2k_x/(k_x'+k_x)$ and $k_x'=[2E+(k_y+1)^2]^{1/2}$. Numerical results for T are shown in Fig. 17(a).

For a Dirac electron the Hamiltonian is given by Eq. (2) with the upper (lower) off-diagonal elements shifted, respectively, by $A(x)$ and $-A(x)$. Looking again for solutions in the form of Eq. (3) we obtain

$$-i\{d/dx+[k_y+A(x)]\}b=Ea, \tag{37a}$$

$$-i\{d/dx-[k_y+A(x)]\}a=Eb. \tag{37b}$$

For $x<0$ and $E^2-k_y^2>0$ the solution for a and b is

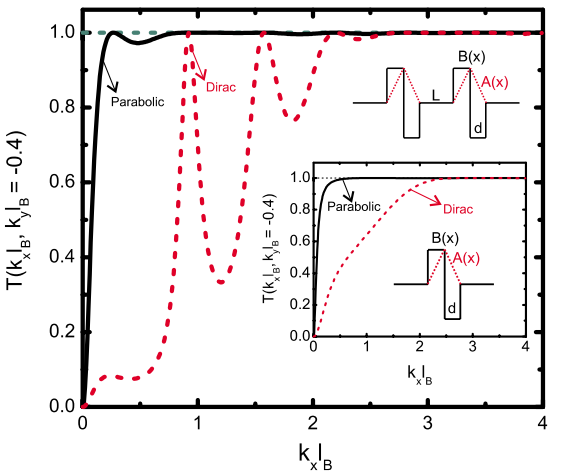

FIG. 15. (Color online) Transmission probability for a Dirac electron and a standard electron. The structure shown in the upper inset has $d=l_B$ and $L=3l_B$. The lower inset shows the corresponding transmission through a single unit.

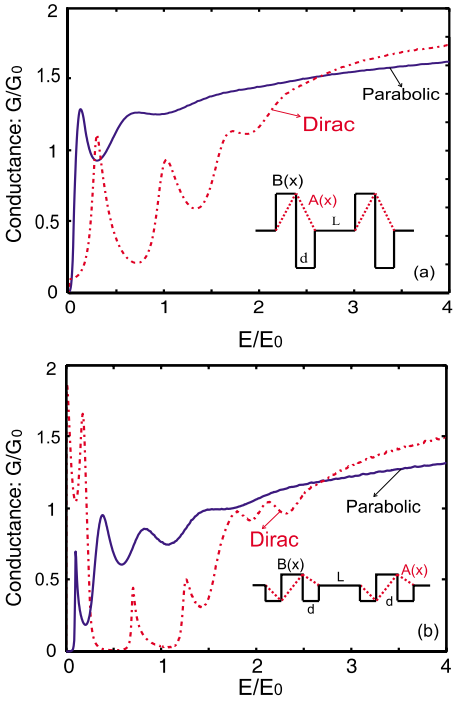

FIG. 16. (Color online) A comparison of the conductance through two complex barrier structures, shown in the insets, for Dirac electrons ($E_0=\hbar v_F/\ell_B$) and standard electrons ($E_0=\hbar\omega_c$). The structures are characterized by $d=l_B$ and $L=3l_B$.

$$a(x)=e^{ik_x x}+re^{-ik_x x}, b(x)=e^{ik_x x+i\phi}-re^{-ik_x x-i\phi}, \tag{38}$$

where $\tan\phi=k_y/k_x$. For $x>0$ the result is

$$a(x)=te^{ik_x' x}, b(x)=te^{ik_x' x+i\theta}. \tag{39}$$

With $\tan\theta=(k_y+1)/k_x'$ the transmission coefficient is

$$t=2\cos(\phi)/(e^{i\theta}+e^{-i\phi}). \tag{40}$$

where $E=\pm[k_x'^2+(k_y+1)^2]^{1/2}$. Then the continuity of the wave function gives the transmission probability

$$T=(k_x'/k_x)|t|^2. \tag{41}$$

A contour plot of this transmission probability is shown in Fig. 17(b). Notice that Dirac electrons have a smaller window for $T\approx 1$ transmission as compared to the standard electrons. There are no qualitative differences between the results for a δ-function barrier [Fig. 17(b)] and those for a barrier of finite width (Fig. 4).

We know that a δ-function potential well has one bound state. Let us investigate if a δ-function magnetic barrier has any bound state. If it does, it is expected to occur for $k_y^2>E^2$. For $x<0$ the wave function is

$$\psi(x)\sim e^{ik_y y}e^{k_x x}\begin{pmatrix} 1 \\ (-i/E)(k_x-k_y^-) \end{pmatrix}, \tag{42}$$

while for $x>0$ there is a constant vector potential; with $k_y^{\pm}=k_y\pm 1/2$ the wave function is

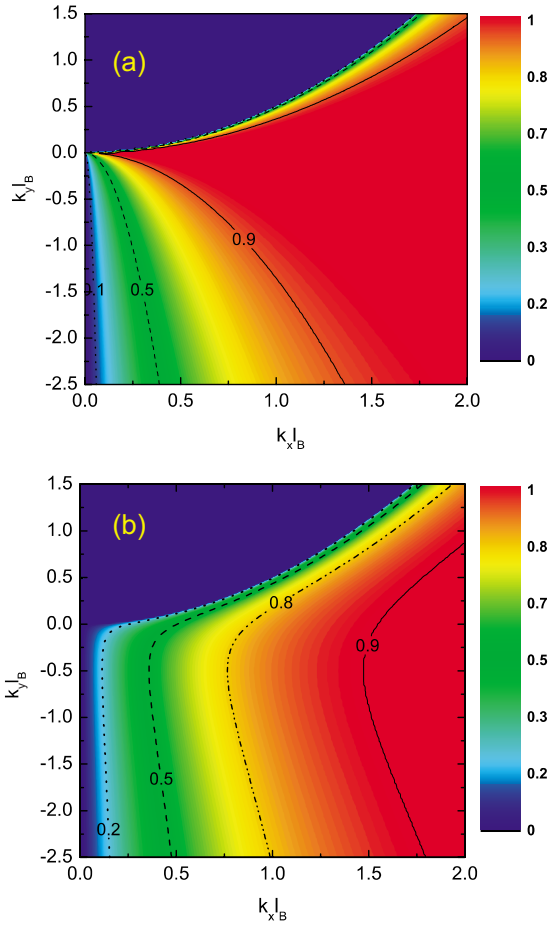

FIG. 17. (Color online) Contour plot of the transmission probability through a magnetic δ-function barrier for (a) a standard electron and (b) a Dirac electron.

$$\psi(x) \sim e^{ik_y y} e^{-k'_x x} \begin{pmatrix} 1 \\ (i/E)(k'_x + k_y^+) \end{pmatrix}. \tag{43}$$

Matching the wave functions at $x=0$ we obtain

$$[(k_y^+)^2 - E^2]^{1/2} + [(k_y^-)^2 - E^2]^{1/2} + 1 = 0. \tag{44}$$

This equation cannot be satisfied and therefore a magnetic δ-function barrier does not have any bound states. We now consider the special case $E=0$. For $x<0$ Eqs. (5a) and (5b) give $(d_-=b, d_+=a)$,

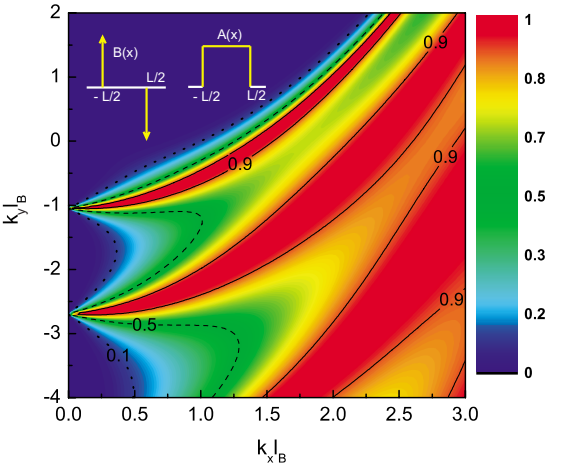

FIG. 18. (Color online) Contour plot of the transmission probability through two opposite δ-function barriers, see inset, with $L=4l_B$.

$$(k_x \mp ik_y^-) d_\mp = 0, \tag{45}$$

The wave function with $a=0, b\neq 0$ is

$$\Psi_I \sim e^{ik_y y} e^{-k_y^- x} \begin{pmatrix} 0 \\ 1 \end{pmatrix}. \tag{46}$$

For $x<0$ Eq. (46) can be a solution if $k_y^-<0$. In the region $x>0$ Eqs. (5a) and (5b) become

$$(k'_x \mp ik_y^+) d_\mp = 0. \tag{47}$$

The corresponding wave function is

$$\Psi_{II} \sim e^{ik_y y} e^{-k_y^+ x} \begin{pmatrix} 0 \\ 1 \end{pmatrix}. \tag{48}$$

In order to have a proper solution for $x>0$ it is convenient to choose $k_y^+>0$. Thus we have a line of bound states with $E=0$ and $-1/2<k_y<1/2$.

For a *resonant tunneling structure*, consisting of two δ-function magnetic barriers, we can combine the results for two single barriers and obtain the transmission through the structure. Solving $H\Psi=E\Psi$ we obtain

$$A(x,y) = \begin{cases} e^{ik_x x + ik_y y} + re^{-ik_x x + ik_y y} & x < -L/2 \\ ae^{ik'_x x + ik_y y} + be^{-ik'_x x + ik_y y} & |x| \le L/2 \\ te^{ik_x x + ik_y y} & x > L/2 \end{cases}, \tag{49}$$

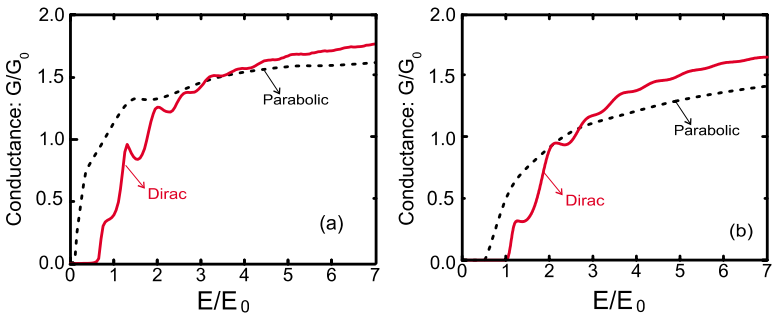

FIG. 19. (Color online) (a) The conductance through *one* δ-function barrier with $L=4l_B$ for a Dirac electron (solid red curve) and a standard electron (dashed black curve) with $E_0=\hbar\omega_c$. (b) As in (a) but for *two* δ-function barriers with the magnetic field in the same direction.

$$B(x,y) = \begin{cases} e^{ik_x x + ik_y y + i\phi} - re^{-ik_x x + ik_y y - i\phi} & x < -L/2 \\ ae^{ik'_x x + ik_y y + i\theta} - be^{-ik'_x x + ik_y y - i\theta} & |x| \le L/2 \\ te^{ik_x x + ik_y y + i\phi} & x > L/2 \end{cases}. \tag{50}$$

Matching the solutions at $-L/2$ and $L/2$ gives

$$t = \frac{2\cos\phi\cos\theta e^{-ik_x L}}{e^{-ik'_x L}[\cos(\theta+\phi)+1] + e^{ik'_x L}[\cos(\theta-\phi)-1]}. \tag{51}$$

Here $k_x = [E^2 - k_y^2]^{1/2}$, $k'_x = [E^2 - (k_y+1)^2]^{1/2}$, $\tan\phi = k_y/k_x$, and $\tan\theta = (k_y+1)/k'_x$. A contour plot of the transmission probability, through two opposite δ-function barriers, is shown in Fig. 18. The transmission exhibits a clear resonant behavior which has a qualitatively different (k_y, k_x) dependence than that of the resonant structures shown in Figs. 18, 12, and 14. When we interchange the sign of the two barriers, i.e., $B \to -B$, we obtain the same transmission with $k_y \to -k_y$.

For two successive δ-function barriers with the magnetic field in the same direction, we obtain $(\theta_\pm = \theta \pm k'_x L)$

$$t = \frac{2\cos\phi\cos\theta e^{-i(k_x + k''_x)L/2}}{e^{i\eta}\cos(\theta_-) + e^{-i\phi}\cos(\theta_+) - (1 + e^{i(\eta-\phi)})i\sin k'_x L}. \tag{52}$$

Here $k''_x = [E^2 - (k_y+2)^2]^{1/2}$ and $\tan\eta = (k_y+2)/k''_x$. A contour plot of the transmission is shown in Fig. 20 and the conductance in Fig. 19(b). The transmission in Fig. 20 has some similarity with the finite-width barrier result shown in Fig. 7; the difference here is that resonances are more pronounced and their number is increased.

V. CONCLUDING REMARKS

We evaluated the transmission through various magnetic-barrier nanostructures based on graphene. In particular, we treated in detail a magnetic step, single and double regular or δ-function barriers, as well as complex structures with inhomogeneous magnetic-field profiles but such that the average magnetic field vanishes.

We obtained bound states that are localized near the magnetic step or the edges of the regular barriers but not for δ-function barriers. Our results agree with the limited ones, for a single barrier in Ref. 15 and a step in Ref. 15, but importantly they differ in the $E=0$ bound state which was not obtained in Ref. 15. In addition, we showed that the transmission exhibits a strong dependence on the direction of the incident electron or hole wave vector. In general, the resonant structure of the transmission is significantly more pronounced for Dirac electrons with *linear* spectrum than for those with a *parabolic* spectrum. Moreover, the transmission through the complex structures of Sec. V shows a much more pronounced resonance than that through single or double barriers. To our knowledge these results are new.

An important feature of the transmission results is their dependence on the angle of incidence as shown in several figures and highlighted in Ref. 15 for a single barrier: the transmission is finite only in a certain range of angles of incidence, shown for a single barrier schematically in Fig. 3 and more explicitly in Fig. 5. One can further modify the angular dependence of the transmission with double barriers (cf. Fig. 9). The main parameters that control this angular dependence are the width of the barriers and/or wells and the energy of the incident electrons.

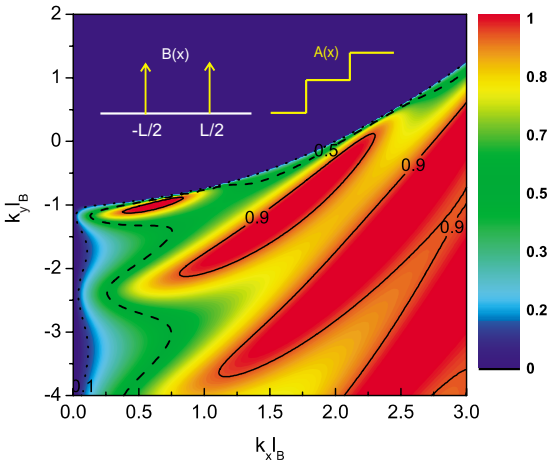

FIG. 20. (Color online) Contour plot of the transmission probability for two δ-function barriers in the same direction with $L = 4l_B$. The inset shows the magnetic-field and vector potential profiles.

A further aspect of our results for graphene-based nanostructures, involving electrons with a nearly *linear* spectrum, is their contrast with those for standard electrons characterized by a *parabolic* spectrum[14] (see Figs. 8, 13, 15, 16, and 19). We saw a marked difference not only in the transmission but also in its average over half the Fermi surface, that is, the conductance given by Eq. (9) (see Figs. 16 and 19). The resonant behavior, especially for double barriers, is significantly more pronounced for electrons with a nearly *linear* spectrum. The behavior of the conductance shown in Fig. 19, for a *linear* spectrum, is similar to that through a double barrier created by two ferromagnetic stripes placed above a graphene layer.[20]

Given the rapid progress in the field and the quest for carbon-based nanostructure devices, we expect that the predictions and/or findings of this paper will be tested experimentally in the near future. We defer to future work the influence of spin and spin-orbit interaction in transport through these or similar graphene nanostructures.

ACKNOWLEDGMENTS

This work was supported by the Flemish Science Foundation (FWO-Vl), by the Belgian Science Policy (IAP), and by the Canadian NSERC Grant No. OGP0121756. Discussions with A. Ludu are gratefully acknowledged.

*takis@alcor.concordia.ca
†amatulis@takas.lt
‡francois.peeters@ua.ac.be

[1] K. S. Novoselov, A. K. Geim, S. V. Morozov, D. Jiang, Y. Zhang, S. V. Dubonos, I. V. Grigorieva, and A. A. Firsov, Science **306**, 666 (2004).
[2] Y. Zhang, Y. W. Tan, H. L. Stormer, and P. Kim, Nature (London) **438**, 201 (2005).
[3] Y. Zheng and T. Ando, Phys. Rev. B **65**, 245420 (2002).
[4] V. P. Gusynin and S. G. Sharapov, Phys. Rev. Lett. **95**, 146801 (2005).
[5] K. S. Novoselov, A. K. Geim, S. V. Morozov, D. Jiang, and M. I. Katsnelson, Nat. Phys. **2**, 177 (2006); E. McCann and V. I. Fal'ko, Phys. Rev. Lett. **96**, 086805 (2006).
[6] O. Klein, Z. Phys. **53**, 157 (1929).
[7] M. I. Katsnelson, K. S. Novoselov, and A. K. Geim, Nat. Phys. **2**, 620 (2006).
[8] J. M. Pereira, Jr., V. Mlinar, F. M. Peeters, and P. Vasilopoulos, Phys. Rev. B **74**, 045424 (2006).
[9] J. Milton Pereira, Jr., F. M. Peeters, and P. Vasilopoulos, Appl. Phys. Lett. **90**, 132122 (2007).
[10] A. K. Geim and K. S. Novoselov, Nat. Mater. **6**, 183 (2007); C. Beenakker, arXiv:0710.3848 (unpublished); A. H. Castro Neto, F. Guinea, N. M. R. Peres, K. S. Novoselov, and A. K. Geim, arXiv:0709.1163, Rev. Mod. Phys. (to be published).
[11] N. M. R. Peres, A. H. Castro Neto, and F. Guinea, Phys. Rev. B **73**, 241403(R) (2006); P. G. Silvestrov and K. B. Efetov, Phys. Rev. Lett. **98**, 016802 (2007).
[12] B. Trauzettel and Denis V. Bulaev, D. Loss, and G. Burkard, Nat. Phys. **3**, 192 (2007).
[13] J. Milton Pereira, Jr., P. Vasilopoulos, and F. M. Peeters, Nano Lett. **7**, 946 (2007).
[14] A. Matulis, F. M. Peeters, and P. Vasilopoulos, Phys. Rev. Lett. **72**, 1518 (1994).
[15] (a) A. De Martino, L. Dell'Anna, and R. Egger, Phys. Rev. Lett. **98**, 066802 (2007); (b) Solid State Commun. **144**, 547 (2007).
[16] L. Oroszlany, P. Rakyta, A. Kormanyos, C. J. Lambert, and J. Cserti, Phys. Rev. B **77**, 081403(R) (2008).
[17] F. M. Peeters and A. Matulis, Phys. Rev. B **48**, 15166 (1993).
[18] S. Park and H.-S. Sim, Phys. Rev. B **77**, 075433 (2008).
[19] I. S. Ibrahim and F. M. Peeters, Phys. Rev. B **52**, 17321 (1995).
[20] F. Zhai and K. Chang, Phys. Rev. B **77**, 113409 (2008).